Role of the Electrophilic Lipid Peroxidation Product 4-Hydroxynonenal in the Development and Maintenance of Obesity in Mice[†]

Sharda P. Singh,[‡,§] Maciej Niemczyk,[‡,§] Deepti Saini,[‡,||] Yogesh C. Awasthi,[⊥] Ludwika Zimniak,[‡] and Piotr Zimniak*[,‡,@]

Department of Pharmacology and Toxicology, University of Arkansas for Medical Sciences, Little Rock, Arkansas 72205, Department of Molecular Biology and Immunology, University of North Texas Health Science Center, Fort Worth, Texas 76107, and Central Arkansas Veterans Healthcare System, Little Rock, Arkansas 72205

Received October 23, 2007; Revised Manuscript Received January 31, 2008

ABSTRACT: The lipid peroxidation product 4-hydroxynonenal (4-HNE) is a signaling mediator with wide-ranging biological effects. In this paper, we report that disruption of *mGsta4*, a gene encoding the 4-HNE-conjugating enzyme mGSTA4-4, causes increased 4-HNE tissue levels and is accompanied by age-dependent development of obesity which precedes the onset of insulin resistance in 129/sv mice. In contrast, *mGsta4* null animals in the C57BL/6 genetic background have normal 4-HNE levels and remain lean, indicating a role of 4-HNE in triggering or maintaining obesity. In *mGsta4* null 129/sv mice, the expression of the acetyl-CoA carboxylase (ACC) transcript is enhanced several-fold with a concomitant increase in the tissue level of malonyl-CoA. Also, mitochondrial aconitase is partially inhibited, and tissue citrate levels are increased. Accumulation of citrate could lead to allosteric activation of ACC, further augmenting malonyl-CoA levels. Aconitase may be inhibited by 4-HNE or by peroxynitrite generated by macrophages which are enriched in white adipose tissue of middle-aged *mGsta4* null 129/sv mice and, upon lipopolysaccharide stimulation, produce more reactive oxygen species and nitric oxide than macrophages from wild-type mice. Excessive malonyl-CoA synthesized by the more abundant and/or allosterically activated ACC in *mGsta4* null mice leads to fat accumulation by the well-known mechanisms of promoting fatty acid synthesis and inhibiting fatty acid β-oxidation. Our findings complement the recent report that obesity causes both a loss of mGSTA4-4 and an increase in the level of 4-HNE [Grimsrud, P. A., et al. (2007) *Mol. Cell. Proteomics 6*, 624–637]. The two reciprocal processes are likely to establish a positive feedback loop that would promote and perpetuate the obese state.

Reactive oxygen species (ROS)[1] initiate a chain reaction in polyunsaturated fatty acids (*1*). The products of this process, lipid hydroperoxides, can be converted (*2, 3*) into a variety of α,β-unsaturated aldehydes of which 4-hydroxynon-2-enal (4-hydroxynonenal or 4-HNE) (*4, 5*) is the most abundant and prototypical example. At physiological concentrations, 4-HNE is a signaling molecule which conveys the information that oxidative stress has occurred and modulates a variety of fundamental biological processes, primarily by forming adducts with proteins and altering their function (reviewed in refs *6–8*). At higher levels, the strongly electrophilic 4-HNE may react indiscriminately with nucleophilic centers of biological macromolecules, leading to toxicity (*4*).

Mitochondrial respiration is the major but not only source of ROS able to trigger lipid peroxidation. Whereas mitochondrial ROS generation is a byproduct of the main reaction (respiration), the pro-inflammatory cells of the innate immune system, such as macrophages, form ROS as part of their normal function. Low-grade but chronic inflammation of the adipose tissue with its accompanying oxidative stress is a hallmark of obesity (*9*); infiltrating macrophages (*10–12*) play a major role in generating the oxidative stress. Accordingly, the white adipose tissue (WAT) of obese mice overproduces 4-HNE (*13*).

Because at least part of the lipid peroxidation process that leads to the formation of 4-HNE is nonenzymatic and thus probably not regulated (*14, 15*), the levels of the compound are biologically determined by its metabolism. By limiting the formation of 4-HNE adducts on proteins, such metabolism has a protective role against 4-HNE toxicity and also serves to terminate 4-HNE-mediated signaling. The metabolism of 4-HNE (reviewed in ref *6*) can be oxidative,

[†] This work was supported in part by National Institutes of Health Grants R01 ES07804 and R01 AG18845 (to P.Z.), P01 AG20641 (to Robert J. Shmookler Reis), and R01 ES 012171 (to Y.C.A.). P.Z. is a recipient of a VA Research Career Scientist Award.

* To whom correspondence should be addressed. E-mail: zimniakpiotr@uams.edu. Telephone: (501) 257-4843. Fax: (501) 257-6439.

[‡] University of Arkansas for Medical Sciences.

[§] These authors contributed equally to this work.

[||] Present address: Department of Surgery, Washington University in St. Louis, St. Louis, MO 63130.

[⊥] University of North Texas Health Science Center.

[@] Central Arkansas Veterans Healthcare System.

[1] Abbreviations: 4-HNE, 4-hydroxynon-2-enal; GST, glutathione transferase; ROS, reactive oxygen species; iNOS, inducible nitric oxide synthase; SDS−PAGE, sodium dodecyl sulfate−polyacrylamide gel electrophoresis; WAT, white adipose tissue; ACC, acetyl-CoA carboxylase; LPS, bacterial lipopolysaccharide; PBS, phosphate-buffered saline; MCP-1, monocyte chemoattractant protein-1; CPT1, carnitine palmitoyltransferase-1; OA, oxaloacetate; AMPK, AMP-activated protein kinase; TCA cycle, tricarboxylic acid cycle; SD, standard deviation.

10.1021/bi702124u CCC: $40.75
Published on Web 03/01/2008

reductive, or conjugative. The latter reaction, i.e., Michael adduct formation with glutathione, is one of the many catalytic and noncatalytic activities of glutathione transferases (GSTs), a superfamily of ancient and versatile enzymes (*16, 17*). In particular, the mGSTA4-4 isoform has, among murine GSTs, the highest catalytic efficiency for 4-HNE (*18–24*) and was therefore targeted for disruption (*25*) to study the biological roles of 4-HNE in the context of the intact organism. In this work, we report that the biochemical phenotype of *mGsta4* null mice is strain-dependent: *mGsta4* null animals in the 129/sv genetic background have elevated tissue levels of 4-HNE, while those in the C57/BL6 genetic background maintain normal, or near-normal, levels of 4-HNE. While the reasons for this differential effect of *mGsta4* disruption in these two strains are not clear, we have utilized this interesting model system to explore the interrelation between 4-HNE levels and obesity, a striking physiological end point we observed. We report that *mGsta4* null mice with an increased level of 4-HNE (129/sv genetic background) are obese, whereas *mGsta4* null animals with unchanged 4-HNE (C57BL/6 background) are not and thus constitute a powerful control. Furthermore, we describe possible biochemical mechanisms through which 4-HNE may contribute to an increased level of fat storage. Finally, we note that our finding (obesity triggered by an elevated tissue level of 4-HNE) complements the published results of Grimsrud et al. (*13*) that diet-induced obesity leads to a loss of mGSTA4-4 and to an increased level of 4-HNE. On the basis of the reciprocal relationship between 4-HNE and obesity, we propose a hypothesis of how 4-HNE-linked biochemical processes may contribute to a self-sustaining nature of the obese state.

EXPERIMENTAL PROCEDURES

Animals. Mice lacking a functional gene encoding mGSTA4-4 (*mGsta4* null animals) in both 129/sv and C57BL/6 genetic backgrounds were obtained as previously described (*25*). Locally maintained breeding colonies of wild-type and homozygous *mGsta4* null mice in both genetic backgrounds were used to generate experimental animals. All mice had ad libitum access to water and to Harlan Teklad LM-485 Mouse/Rat Sterilizable Diet. The genotype of mice with regard to the *mGsta4* gene was occasionally confirmed by a PCR method using tail biopsy samples and the Extract-N-Amp Tissue PCR Kit (Sigma, St. Louis, MO). Multiplex PCRs were carried out using the common sense primer 5′-tccaatacacaaaaatgcatga, the antisense primer 5′-gatggccctg-gtctgtgtcagc specific for the wild-type *mGsta4* allele, and the antisense primer 5′-ctgtccatctgcacgagactagtg derived from the *neo* cassette and thus specific for *mGsta4* null animals. After 33 PCR cycles at an annealing temperature of 56 °C, a product of 284 bp was obtained for wild-type animals and a product of 543 bp for *mGsta4* null animals.

Experiments on animals were performed in accordance with a protocol approved by the Institutional Animal Use and Care Committee.

Blood Glucose Measurements and Glucose Tolerance and Insulin Sensitivity Tests. For fasting blood glucose determinations, mice were fasted for 8 h, a drop of blood was obtained from a tail nick, and the glucose level was measured using TheraSense test strips and a FreeStyle Flash reader (TheraSense, Alameda, CA). For glucose tolerance and insulin sensitivity tests, animals were fasted for 4 h and a baseline level of glucose was determined as described above. A 20% (w/w) solution of glucose in 0.15 M NaCl or 0.1 unit/mL of human insulin in 0.15 M NaCl was injected intraperitoneally until a level of 2 g of glucose/kg of body weight or 0.75 unit of insulin/kg of body weight, respectively, was reached. The blood glucose level was then measured as described above at postinjection times indicated in the individual experiments.

Determination of Tissue Levels of 4-HNE. Malondialdehyde and 4-HNE were determined colorimetrically according to the method of ref *26* with slight modifications. Mouse tissues were quick-frozen using Wollenberger tongs (two large blocks of aluminum that are precooled in liquid nitrogen and can be brought together rapidly; (*27*)). For each determination, 20% (w/v) homogenates of the frozen tissues were prepared in 20 mM potassium phosphate buffer (pH 7.0) containing 5 mM butylated hydroxytoluene, using a Polytron PT3000 apparatus equipped with a PT/DA 3007/2 probe (Brinkmann, Westbury, NY). The homogenates were centrifuged at 3000*g* for 15 min, and the protein concentration was determined using the Bradford reagent (Bio-Rad, Hercules, CA). To each 200 μL sample were added 650 μL of 10 mM *N*-methyl-2-phenylindole and 150 μL of either 12 N HCl (for determination of the malondialdehyde concentration) or 15.4 M methanesulfonic acid (for determination of the sum of 4-HNE and malondialdehyde concentrations). The reaction mixtures were vortexed and incubated at 45 °C for 60 min. After centrifugation at 15000*g* for 10 min, the absorbance of the supernatants was determined at 586 nm. Standards of malondialdehyde and 4-HNE were prepared by hydrolysis of 1,1,3,3-tetramethoxypropane or of 4-HNE dimethylacetal in 1 mM HCl or 1 mM methanesulfonic acid, respectively, for 1 h at room temperature. 4-HNE dimethylacetal was synthesized according to the methods of Gree et al. (*28*) and Chandra and Srivastava (*29*). The concentration of 4-HNE was calculated by subtracting the malondialdehyde concentration from the experimentally determined sum of 4-HNE and malondialdehyde.

Determination of the Malonyl-CoA Concentration in Tissues. Mouse tissues were quick-frozen using Wollenberger tongs as described in the previous section and were stored at –75 °C. Tissue fragments were weighed, and approximately 0.1−0.2 g of tissue was homogenized in 2 mL of extraction buffer [3:1 (v/v) acetonitrile/10 mM potassium phosphate mixture (pH 7.4)] by three 10 s bursts of a Polytron PT3000 homogenizer equipped with a PT/DA 3007/2 probe (Brinkmann, Westbury, NY). The homogenates were further diluted to 7 mL using same extraction buffer and kept on ice for 30 min with intermittent vortexing. Precipitated protein was then pelleted by centrifugation at 20000*g* for 10 min, and the supernatant was collected. The pellet was re-extracted as described above, and supernatants were combined. The pooled supernatants were mixed with 2 volumes of chloroform and vortexed vigorously for approximately 1 min. Phases were separated by centrifugation in a swing-out rotor for 5 min at 4000*g*, and the aqueous phase was collected. The organic phase was re-extracted with 1 mL of 10 mM potassium phosphate (pH 7.4), and the combined aqueous phases were passed though Discovery DSC-18 solid phase extraction column (size, 100 mg/1 mL;

Suppelco/Sigma, St. Louis, MO) according to the manufacturer's instructions. The column was eluted with 2 × 1 mL of acetone; the eluate was dried under nitrogen, and the residue was reconstituted in a 95:5 (v/v) 10 mM potassium phosphate (pH 7.4)/methanol mixture and stored at −70 °C until use. HPLC was performed on a Waters 2695 separations module fitted with a Waters 996 PDA detector and a 25 cm × 4.6 mm Discovery C18 column (5 μm particle size, 180 Å pore size), protected by a guard column (Suppelco); data were acquired and analyzed using Empower 2. Chromatography was carried out using two buffers. Buffer A consisted of 10.5 mM tetrabutylammonium hydroxide, 10.5 mM potassium phosphate (pH 7.0) (95%), and methanol (5%), and buffer B consisted of 4.3 mM tetrabutylammonium hydroxide, 92.3 mM potassium phosphate (pH 5.0) (65%), and methanol (35%). The following gradient was used (all at a flow rate of 0.9 mL/min): 100% buffer A from 0 to 2 min, linear gradient from 100 to 45% buffer A from 2 to 40 min, linear gradient from 45 to 41% buffer A from 40 to 44 min, linear gradient from 41 to 10% buffer A from 44 to 75 min, linear gradient from 10 to 8% buffer A from 75 to 77 min, 8% buffer A from 77 to 83 min, linear gradient from 8 to 0% buffer A from 83 to 93 min, 0% buffer A from 93 to 113 min, and linear gradient from 0 to 100% buffer A from 113 to 120 min (in all steps, the sum of buffer A and buffer B was 100%). The malonyl-CoA peak was initially identified by comparing the retention time and the absorption spectrum with those of a freshly prepared solution of authentic malonyl-CoA (Sigma). More conclusive identification was obtained by cochromatography after spiking biological samples with authentic malonyl-CoA prior to workup. The chromatography conditions described above are derived from those of Lazzarino (*30*) but were modified to optimize the separation of the malonyl-CoA peak from other metabolites.

Determination of Citrate Levels in Tissues. Citrate was assessed by a coupled enzyme assay utilizing citrate lyase and malate and lactate dehydrogenases (*31*), as implemented in the citric acid determination kit by Boehringer Mannheim/R-Biopharm (Roche, Marshall, MI). Tissues were quick-frozen using Wollenberger tongs and were pulverized in liquid nitrogen prior to homogenization in 1 M perchloric acid. Following centrifugation, the supernatant was neutralized and used for the assay as recommended by the manufacturer.

Real-Time RT-PCR for Determination of Acc2 and Cd68 Transcript Levels. Total RNA was isolated from liver and skeletal muscle by the guanidinium thiocyanate method (*32*) using 1 mL of TRI Reagent (Molecular Research Center, Cincinnati, OH) per 20 mg of frozen tissue. RNA from WAT (50 mg of tissue) was isolated using a RNeasy Lipid Tissue Mini Kit (Qiagen, Valencia, CA) according to the manufacturer's instructions. First-strand cDNA synthesis was carried out with the QuantiTect Reverse Transcription Kit (Qiagen) following DNase treatment of the RNA; a mixture of oligo(dT) and random hexamer primers was used. Real-time quantitative PCR amplification reactions were performed with the FastStart SYBR Green Master mix (Roche Diagnostics, Indianapolis, IN) in a total volume of 25 μL using 0.3 μM gene-specific primers. For *Cd68* (macrosialin), the sense primer was 5′-tacaggctgctcagctgcctgac and the antisense primer was 5′-atgcagaaggcgatgagcaccag (product length of 139 bp). Primer sequences for *Acc2* (*Acacb*) were obtained from PrimerBank (http://pga.mgh.harvard.edu/primerbank; (*33*)). Specifically, primer pair entry 18606146a1 was used (sense primer 5′-cctttggcaacaagcaaggta, antisense primer 5′-agtcgtacacataggtggtcc, product length of 123 bp). mRNA encoding the S3 ribosomal protein was used as the reference (PrimerBank entry 6755372a2; sense primer 5′-ttacaccaacaggacagaaatc, antisense primer 5′-tggacaactgcggtcaactc, product length of 100 bp). The S3 transcript was found to be suitable as a normalizer for these studies because in preliminary experiments it was shown to be invariant between livers of wild-type and *mGsta4* null 129/sv mice (data not shown). Amplifications were performed using the DNA Engine Opticon 2 Detection System (MJ Research, Waltham, MA) as follows: 50 °C for 2 min, initial denaturation at 95 °C for 10 min, followed by 40 cycles of 95 °C for 15 s, 61 °C for 30 s, and 72 °C for 30 s.

Isolation of Skeletal Muscle and Liver Mitochondria and Determination of Aconitase Activity. Mitochondria from skeletal muscle were isolated according to the method of Rebrin and Sohal (*34*). Briefly, a 10% (w/v) tissue homogenate in 0.12 M KCl, 2 mM $MgCl_2$, 1 mM EGTA, 0.5 mg/mL bovine serum albumin, and 20 mM Hepes (pH 7.4) was prepared on ice by four 10 s bursts of a Polytron PT3000 apparatus equipped with a PT/DA 3007/2 probe (Brinkmann) and operated at 15000 rpm. The homogenate was centrifuged for 12 min at 600*g*, and the supernatant was recentrifuged for 12 min at 16000*g*. The pellet was resuspended in the original volume of 0.3 M sucrose, 0.1 mM EGTA, and 2 mM Hepes (pH 7.4) and centrifuged for 12 min at 12000*g*. The final pellet was resuspended in 0.3 M sucrose, 0.1 mM EGTA, and 2 mM Hepes (pH 7.4) at one-tenth of the original volume. Liver mitochondria were prepared also according to the method of Rebrin and Sohal (*34*). Briefly, a 10% (w/v) liver homogenate in 0.25 M sucrose, 3 mM EDTA, and 10 mM Tris-HCl (pH 7.4) was prepared on ice by three 10 s bursts of a Polytron PT3000 apparatus equipped with a PT/DA 3007/2 probe (Brinkmann) and operated at 15000 rpm. The homogenate was centrifuged for 11 min at 600*g*, and the supernatant was centrifuged for 10 min at 10000*g*. The pellet was resuspended in the original volume of the buffer described above, and the two centrifugations were repeated. The final pellet was resuspended in 0.25 M sucrose at one-tenth of the original volume. Aconitase activity was determined according to the method of ref *35* by incubating mitochondria in 90 mM Tris-HCl (pH 8.0) and 20 mM isocitrate for 5 min at 30 °C and recording the absorbance at 240 nm; the extinction coefficient for aconitate is 3.6 mM^{-1} cm^{-1} (*36*).

Isolation of Peritoneal Macrophages, LPS Challenge, and Determination of Nitric Oxide and ROS Levels. Mice were treated intraperitoneally with 1 mL of 3% thioglycolate medium (Sigma) in phosphate-buffered saline (PBS). Two days later, macrophages were obtained. The mouse was lightly anesthetized with CO_2, and the abdomen was cleaned with 70% alcohol. Five milliliters of DMEM with penicillin/streptomycin was injected into the peritoneum through a 21-gauge needle, and the peritoneal wash was withdrawn. The procedure was repeated, and the macrophage-containing washes were combined. Cells were pelleted by centrifugation at 800*g* for 5 min, resuspended is DMEM supplemented with 10% fetal bovine serum, counted, and plated at a density of

1×10^5 cells/well in a 96-well plate. After 2 h at 37 °C, nonadherent cells were washed off. Fresh medium was added, and attached cells were incubated overnight. The medium was then replaced with phenol red-free DMEM supplemented with 10% fetal bovine serum, penicillin/streptomycin, and 100 ng/mL LPS. After incubation at 37 °C for the time periods specified in the individual experiments, the supernatant was withdrawn for determination of nitric oxide levels using the Griess reagent and a nitrite standard curve as described in ref *37*, and cells were assayed for ROS. For the latter measurement, cells were washed once with PBS, and 100 μL of PBS was added to each well. After 15 min at 37 °C, 2.5 μL of a 1 mM working solution of 2,7-dihydrodichlorofluorescein diacetate in PBS (freshly diluted from a 10 mM stock in DMSO) was added. After incubation for 30 min at 37 °C, the cells were washed with PBS and fluorescence was measured at an excitation wavelength of 485 nm and an emission wavelength of 525 nm.

RESULTS

mGsta4 Null Mice in the 129/sv but Not the C57BL/6 Genetic Background Are Obese. In our original characterization of *mGsta4* null mice in the 129/sv genetic background (*25*), we found that 4-month-old knockout animals had a slightly higher body weight than wild-type controls (26.5 and 25.4 g, respectively), but the difference was statistically not significant. Examination of additional animals and following their weight as a function of time has demonstrated that *mGsta4* null 129/sv mice are indeed, on average, heavier than matched wild-type mice, as shown in Figure 1A. Growth of mammals is closely approximated by the monomolecular function (*38*). Nonlinear fitting was used to obtain the two parameters of the monomolecular function, maximal weight and the proportionality (growth) parameter, for each individual mouse. The maximal weight was significantly ($P < 0.00002$) greater for female 129/sv *mGsta4* null than for 129/sv wild-type animals, but the proportionality parameter, a measure of the time needed to reach maximal weight, was not different between the two groups (the statistical tests are presented in the legend of Figure 1). The growth trajectories of the two groups of mice can be visualized by plotting the monomolecular function using averaged parameters for each group (lines in Figure 1A). The plot illustrates that, on average, fully grown female *mGsta4* null mice are heavier by approximately 22% than wild-type controls. The effect of the *mGsta4* knockout on the body weight of male mice was similar (18% increase in maximal body weight, $P = 0.0002$; data not shown).

In contrast to the 129/sv strain, the growth curves of wild-type and *mGsta4* null mice in the C57BL/6 genetic background do not differ from each other (Figure 1B).

The increased body weight of *mGsta4* null 129/sv mice is at least partially due to an increased adiposity. As shown in Figure 1C, there was a marked accumulation of fat in the abdominal cavity of *mGsta4* null animals. Dissection of a well-defined male rodent fat depot, the epididymal fat pad, confirmed the increased adiposity of *mGsta4* null mice (Figure 1D). The visual assessment of greater adiposity was validated by dissection and recording the weight of perigonadal fat pads in multiple animals. While there was considerable variability between individual mice, on average the size

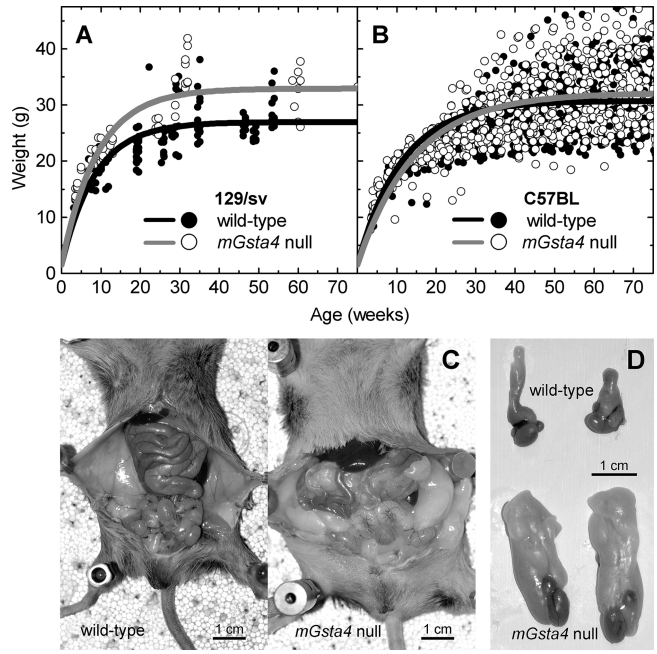

FIGURE 1: Body weight of wild-type and *mGsta4* null female mice in 129/sv (A) and C57BL/6 (B) genetic backgrounds, and visceral fat accumulation in *mGsta4* null male 129/sv animals (C and D). Weights of mice were recorded at different ages [(○) *mGsta4* null mice and (●) wild-type mice; (A) 129/sv and (B) C57BL/6]. The numbers of *mGsta4* null and wild-type animals examined were 21 and 53, respectively, for the 129/sv background and 47 and 49, respectively, for the C57BL/6 genetic background. For each individual mouse, the monomolecular function (*38*) was fitted to the data by nonlinear regression, yielding the maximal weight and the proportionality (growth rate) parameters. The means of the corresponding parameters within each experimental group were used to plot the average growth trajectory of that group [(black line) wild-type and (gray line) *mGsta4* null animals]. By Hotelling's T2 test, the maximal attainable weight parameter of the monomolecular model differs between wild-type and knockout 129/sv mice ($P < 0.00002$) whereas the growth rate parameter is not significantly different ($P = 0.54$). By the same Hotelling's T2 statistical test, the growth trajectories of *mGsta4* null and wild-type C57BL/6 mice do not differ from each other ($P = 0.1$). (C) Composite image showing a preponderance of adipose tissue in the abdominal cavity of a representative 40-week-old male *mGsta4* null 129/sv mouse (left) as compared with an age-, sex-, and strain-matched wild-type control (right). (D) Epididymal fat pads dissected from the mice shown in panel C.

of the epididymal (males) or periovarian (females) fat pads increased with age faster in *mGsta4* null animals than in wild-type mice not only in terms of absolute weight but also when expressed as a percentage of total body mass (Figure 2). The increase appeared to be due to cell size rather than cell number. As shown in Figure 3, adipocytes in *mGsta4* null 129/sv mice had a larger diameter than adipocytes obtained from corresponding wild-type animals. Scoring of the diameter of 50 cells each from three wild-type and four knockout mice after collagenase digestion of adipose tissue indicated that the volume of cells from *mGsta4* null animals was 2.9-fold greater than that of cells from wild-type mice.

Fasting Blood Glucose Levels and Glucose Tolerance Are Similar in Wild-Type and mGsta4 Null Mice. The fasting blood glucose level was slightly higher in *mGsta4* null than in wild-type 129/sv mice (Figure 4A), although for both genotypes the glucose level was within or below the normal range for the 129/sv strain (*39–41*). Because the difference in blood glucose levels between wild-type and *mGsta4* null

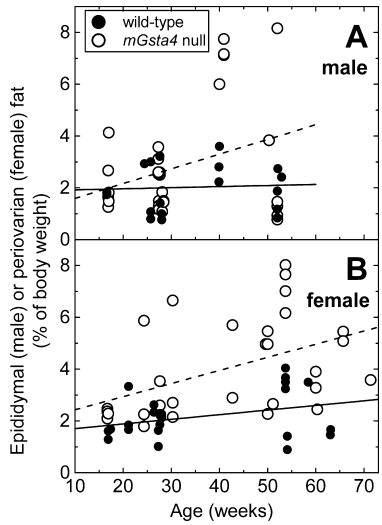

FIGURE 2: Weight of perigonadal fat pads of 129/sv wild-type (filled symbols and solid regression line) and *mGsta4* null (empty symbols and dashed regression line) as a function of age: (A) epididymal fat in male mice and (B) periovarian fat in female mice. In both male and female wild-type mice, the weight of perigonadal fat, expressed as the percentage of total body mass, does not change with age within the age bracket studied ($P = 0.81$ and 0.12, respectively). In *mGsta4* null animals, the increase in the relative weight of epididymal fat with age is suggestive ($P = 0.09$) and the increase in the relative weight of periovarian fat is statistically significant ($P = 0.009$).

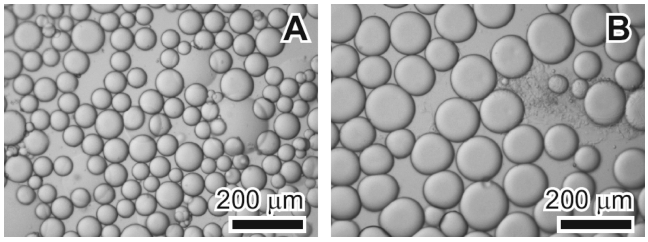

FIGURE 3: Comparison of adipocyte size in periovarian fat of 18-week-old wild-type (A) and *mGsta4* null (B) 129/sv mice. Adipocytes were dispersed by collagenase treatment. The diameter was scored for 50 cells each from three wild-type and four *mGsta4* null mice. Comparison of the mean adipocyte diameters characteristic of the individual mice indicates a significant difference between wild-type and *mGsta4* null animals ($P = 0.006$ by a *t* test).

animals was modest, it was not always evident and was even reversed in some experiments, especially those utilizing small sample sizes (for example, time zero in Figure 4B).

An intraperitoneal glucose tolerance test was performed on wild-type and *mGsta4* null 129/sv mice. The response was identical in young (16-week-old) animals (Figure 4B). In 50-week-old mice, blood glucose levels in response to glucose injection appeared slightly higher in *mGsta4* null than in wild-type animals (Figure 4C). However, the difference was not significant at any of the time points except for 120 min. Integration of the area under the wild-type and *mGsta4* null curves from 0 to 120 min yielded results that were not significantly different (Figure 4D). Therefore, within the precision of the measurements, our data are consistent with the null hypothesis that 129/sv wild-type and *mGsta4* null mice do not differ in glucose tolerance.

mGsta4 Null 129/sv Mice Develop Insulin Resistance with Age. The response of 16-week-old wild-type and *mGsta4* null 129/sv mice to intraperitoneal injection of insulin was similar (Figure 5A,B), indicating that disruption of the *mGsta4* gene had no effect on the insulin sensitivity of the animals at this age. At 50 weeks of age, wild-type animals retained normal insulin sensitivity (Figure 5C). In contrast to young mice of both genotypes (Figure 5A,B) and to 50-week-old wild-type animals, 50-week-old *mGsta4* null mice responded to insulin in a highly nonuniform way, ranging from insulin sensitivity that equaled or exceeded that of wild-type animals to complete insulin resistance (Figure 5D).

The Level of 4-HNE Is Elevated in Tissues of 129/sv but Not C57BL/6 mGsta4 Null Mice. As expected, the lower 4-HNE conjugating activity in 129/sv *mGsta4* null versus wild-type mice (*25*) resulted in a higher steady-state tissue level of 4-HNE (Figure 6A). The tissues that were selected for analysis, skeletal muscle, white adipose tissue (WAT), and liver, play a major metabolic role in fat homeostasis. In contrast to 129/sv mice, the difference in 4-HNE concentrations between tissues of C57BL/6 wild-type and *mGsta4* null animals did not reach statistical significance (Figure 6B). Therefore, on the basis of the available data, we cannot reject the null hypothesis that disruption of the *mGsta4* gene has no effect on tissue levels of 4-HNE in C57BL/6 mice.

The Level of Malonyl-CoA Is Increased in Tissues of 129/sv but Not C57BL/6 mGsta4 Null Mice. Malonyl-CoA is the committed precursor of fatty acid synthesis in lipogenic tissues and an allosteric inhibitor of uptake of fatty acids into mitochondria, and thus of fatty acid β-oxidation, in oxidative tissues. For these reasons, an excess of malonyl-CoA leads to fat deposition, whereas low malonyl-CoA levels cause a lean phenotype. The level of malonyl-CoA correlated with the tissue concentration of 4-HNE. In the 129/sv *mGsta4* null mouse, which has an elevated 4-HNE level (Figure 6A), the concentration of malonyl-CoA was also increased in all tissues that were tested (Figure 7A). In contrast, *mGsta4* null mice in the C57BL/6 genetic background had levels of both 4-HNE (Figure 6B) and malonyl-CoA (Figure 7B) that were statistically not significantly different from those of matched wild-type controls.

Taken together, the results presented so far indicate a positive correlation between *mGsta4* gene disruption, elevated 4-HNE levels, an increase in the amount of malonyl-CoA, and obesity in 129/sv but not in C57BL/6 mice. This suggests that these events are, in fact, part of a causal chain that is interrupted in C57BL/6 knockout mice at an early stage, possibly by compensatory overexpression of 4-HNE-metabolizing processes alternative to mGSTA4-4-catalyzed conjugation. While interesting in their own right, these hypothetical compensatory mechanisms preclude the accumulation of 4-HNE and obesity. The C57BL/6 strain is thus crucial for this study because it constitutes a negative control: it rules out the possibility that obesity is a nonspecific consequence of disruption of the *mGsta4* gene and focuses attention on 4-HNE as the likely causative factor. At the same time, however, the absence of an elevated level of 4-HNE precludes the use of *mGsta4* null C57BL/6 mice for mechanistic studies of the process by which an increased level of 4-HNE triggers malonyl-CoA accumulation. For this reason, further studies on possible mechanism(s) leading to obesity in *mGsta4* null mice were carried out with the 129/sv strain.

The Level of Expression of Acc2 mRNA Is Elevated in 129/sv mGsta4 Null Mice. Acetyl-CoA carboxylase (ACC) (*42–46*), the enzyme that catalyzes malonyl-CoA synthesis, plays a

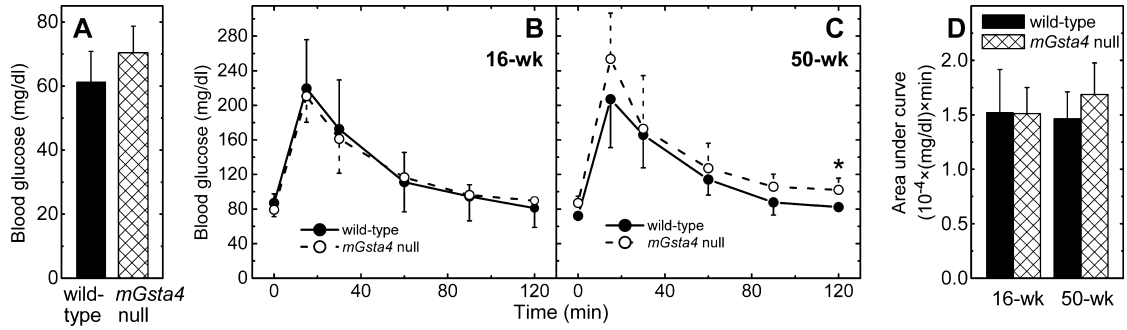

FIGURE 4: Fasting blood glucose levels and glucose tolerance of wild-type (filled symbols or solid bars) and *mGsta4* null (empty symbols or cross-hatched bars) female 129/sv mice. (A) The blood glucose level was measured after an 8 h fasting period in nine wild-type (solid bar) and 13 *mGsta4* null (cross-hatched bar) 16-week-old mice. Means ± SD are shown; the difference between wild-type and *mGsta4* null mice is statistically significant ($P = 0.028$ by a *t* test). (B−D) Animals were fasted for 4 h and were given an intraperitoneal injection of glucose (2 g/kg of body weight). The blood glucose level was determined at the indicated times. Means ± SD of five animals per group are shown; the asterisk indicates a statistically significant difference ($P < 0.05$) between wild-type and *mGsta4* null animals at the time point marked: (B) 16-week-old mice and (C) 50-week-old mice. (D) The area under the blood glucose level vs time curve was calculated by numerical integration between 0 and 120 min for each individual mouse used in panels B and C, and the mean ± SD of the areas is shown. Differences between wild-type and *mGsta4* null mice are not statistically significant ($P = 0.96$ and 0.23 for 16-week-old and 50-week-old animals, respectively, by a *t* test).

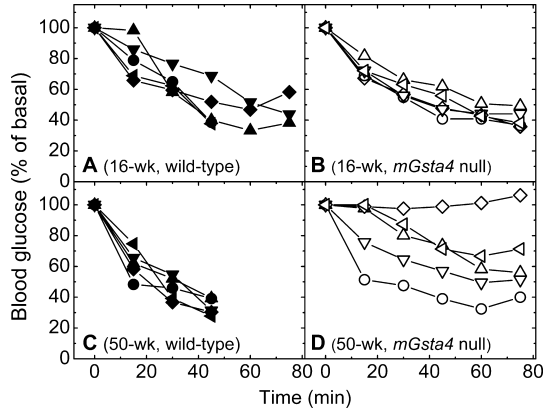

FIGURE 5: Insulin sensitivity of wild-type (filled symbols) and *mGsta4* null (empty symbols) female 129/sv mice. Sixteen-week-old (A and B) and 50-week-old (C and D) wild-type (A and C) and *mGsta4* null (B and D) animals were fasted for 4 h and were given an intraperitoneal injection of human insulin (0.75 unit/kg of body weight). The blood glucose level was determined at the indicated times. Five animals per group were used. Blood glucose levels of individual mice are shown using different plotting symbols.

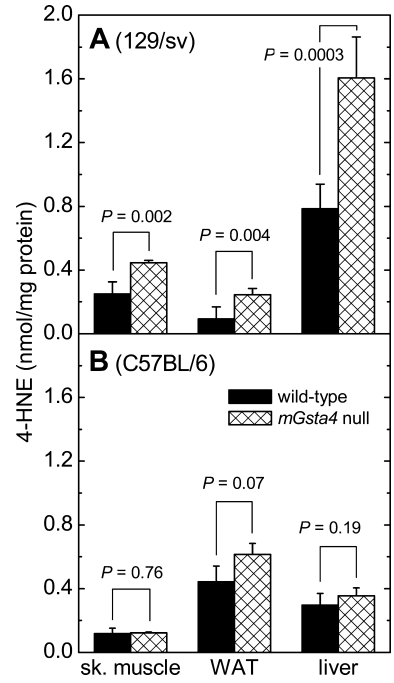

FIGURE 6: 4-HNE level in tissues of 16-week-old female wild-type (solid bars) and *mGsta4* null (cross-hatched bars) mice. The level of 4-HNE was measured as described in Experimental Procedures and in refs *26* and *80*. Means ± SD of five animals per group are shown; the *P* values represent results of *t* tests: (A) 129/sv and (B) C57BL/6.

central role in lipid and energy metabolism of an organism. ACC is tightly regulated via allosteric and phosphorylation signaling pathways that reflect the energy status of the cell. Of the two isoforms of mammalian ACC, mitochondrial ACC2 produces malonyl-CoA whose main biological function is the allosteric inhibition of uptake of fatty acids into mitochondria. As a result, the rate of fatty acid β-oxidation is reduced. We found that the level of expression of the *Acc2* transcript is elevated in skeletal muscle and liver of *mGsta4* null 129/sv mice (Table 1). Transcription is one of the known modalities of ACC regulation (reviewed in ref *44*), and the elevated level of the *Acc2* transcript is likely to lead to more ACC2 protein. Therefore, the increased level of expression of *Acc2* could explain the observed higher concentration of malonyl-CoA in *mGsta4* null mice (Figure 7A).

Mitochondrial Aconitase Activity Is Inhibited in 129/sv mGsta4 Null Mice, and Citrate Levels Are Increased. ACC, and hence the synthesis of malonyl-CoA, is allosterically activated by citrate (*42, 44*). We have therefore determined the activity of aconitase, an enzyme of the tricarboxylic acid (TCA) cycle that metabolizes citrate. In liver, the activity of mitochondrial aconitase was decreased by 22% in *mGsta4* null 129/sv mice compared with matched wild-type controls; the decrease was 14% in skeletal muscle mitochondria (Figure 8). A lower activity of aconitase may result in elevated levels of citrate (*47*). Indeed, direct measurements demonstrated a statistically significant increase in citrate concentrations in skeletal muscle and in liver of young (Figure 9A) and middle-aged (Figure 9B) *mGsta4* null mice. On average, the increase was 60−70% in both tissues.

The Level of Expression of Cd68 mRNA Increases with Age in WAT of mGsta4 Null 129/sv Mice. In WAT of young 129/sv mice, there was no difference in the expression level of the macrophage marker *Cd68* between wild-type and

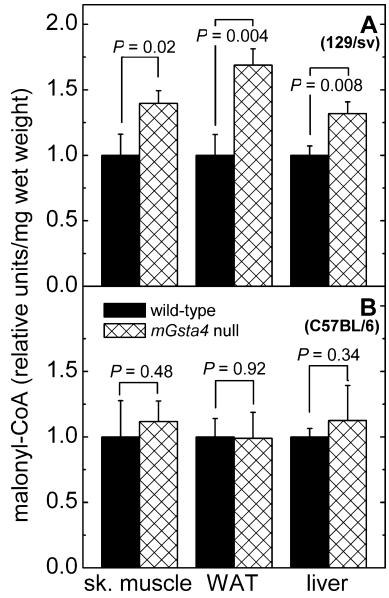

FIGURE 7: Malonyl-CoA level in tissues of 16-week-old female wild-type (solid bars) and *mGsta4* null (cross-hatched bars) mice. The level of malonyl-CoA was measured as described in Experimental Procedures: (A) 129/sv and (B) C57BL/6.

Table 1: Comparison of Levels of Selected Transcripts in Tissues of Wild-Type and *mGsta4* Null Female 129/sv Mice[a]

mRNA encoding	tissue	age	*mGsta4* null/ wild-type ratio	*P*
ACC2	skeletal muscle	16 weeks	3.3 (2.8–3.9)	$<10^{-4}$
	liver	16 weeks	2.1 (1.8–2.5)	0.003
CD68	WAT	16 weeks	1.0 (0.9–1.2)	0.80
	WAT	50 weeks	13.1 (9.7–17.7)	$<10^{-4}$

[a] Transcript levels were measured by reverse-transcription real-time PCR on tissues of five animals per group. Gene expression levels were normalized to the S3 ribosomal protein transcript by calculating for each individual animal the difference, ΔC_t, in the respective cycle numbers. A two-sample *t* test was used to check whether the mean ΔC_t values differ between wild-type and *mGsta4* null mice; the resulting *P* values are listed. The ratio of the gene expression level for *mGsta4* null to wild-type animals was calculated by the $\Delta\Delta C_t$ method (*79*) using an experimentally determined amplification efficiency (typically approximately 1.9). The ratios are listed with confidence intervals corresponding to ±one standard deviation of the $\Delta\Delta C_t$ cycle number.

mGsta4 null animals (Table 1). Strikingly, in older (50-week-old) mice, the level of the *Cd68* transcript was elevated more than 10-fold in knockout relative to wild-type animals (Table 1). There was no significant change in the level of *Cd68* between 16-week-old and 50-week-old wild-type mice ($P = 0.16$; data not shown). Together, these findings suggest a massive age-dependent infiltration of WAT by macrophages in *mGsta4* null mice.

Macrophages from Wild-Type and mGsta4 Null 129/sv Mice Are Differentially Activated. Primary cultures of thioglycolate-elicited peritoneal macrophages from *mGsta4* null animals produced transiently more ROS than wild-type macrophages when treated with LPS (Figure 10A). ROS production was followed by a delayed but more sustained generation of nitric oxide (NO), which again was more pronounced in *mGsta4* null macrophages (Figure 10B). The time course of NO production agreed well with the time course of iNOS induction by LPS (Figure 10C). iNOS was induced in *mGsta4* null macrophages to a level higher than that in wild-type macrophages, in agreement with the greater NO production by the knockout macrophages (Figure 10B).

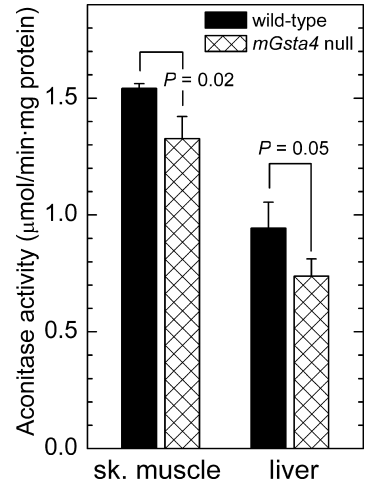

FIGURE 8: Aconitase activity in skeletal muscle and liver mitochondria isolated from wild-type (solid bars) and *mGsta4* null (cross-hatched bars) 129/sv mice (male, 16 weeks old). Mitochondria were isolated according to the method of ref *34*, and aconitase activity was measured as described in ref *35* and in Experimental Procedures. Means ± SD of three animals per group are shown; the *P* values represent the results of *t* tests.

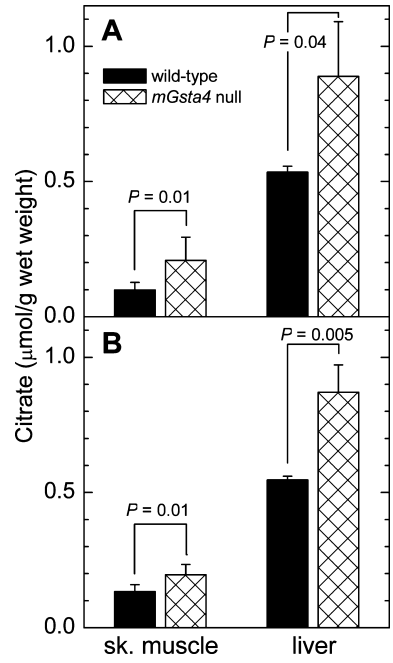

FIGURE 9: Citrate level in skeletal muscle and liver of wild-type (solid bars) and *mGsta4* null (cross-hatched bars) 129/sv female mice that were (A) 17−18 and (B) 47−55 weeks old. Means ± SD of three (for liver) or six (for skeletal muscle) animals per group are shown; the *P* values represent results of *t* tests. Analysis of the data by General Linear Model ANOVA shows that age and the interaction of age with genotype are not significant for either skeletal muscle or liver ($P \geq 0.4$ for both tissues), but the genotype (wild-type vs *mGsta4* null) is significant ($P = 0.04$ for skeletal muscle, and $P = 0.0009$ for liver).

DISCUSSION

The predicted primary effect of disrupting the *mGsta4* gene (*25*) is an elevated concentration of 4-HNE, the substrate of mGSTA4-4. We found the expected increase in tissue levels of 4-HNE in *mGsta4* null mice in the 129/sv but not in the C57BL/6 genetic background. This differential response to disruption of the *mGsta4* gene, while surprising, is nevertheless consistent with the well-known strain dependence of

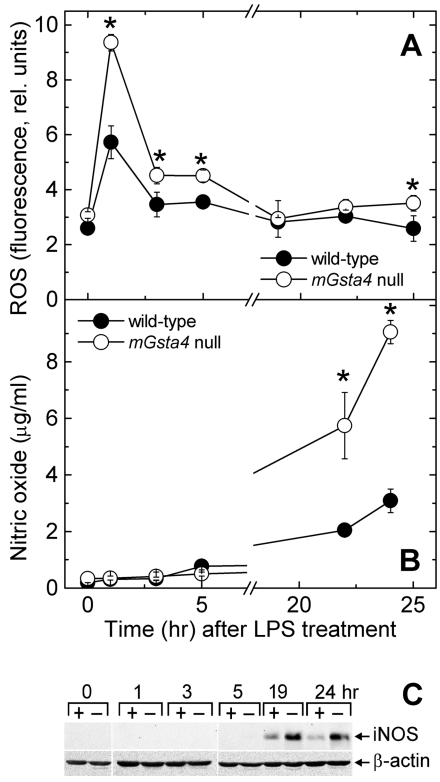

FIGURE 10: Generation of ROS and nitric oxide and induction of iNOS in macrophages from wild-type and *mGsta4* null 129/sv mice. (A and B) Primary cultures of peritoneal macrophages from 11−16-week-old female wild-type (●) and *mGsta4* null (○) mice were treated with LPS (100 ng/mL). After the indicated times, the level of ROS (A) was determined in attached cells and the concentration of nitric oxide (B) was measured in the supernatant. Means ± SD of triplicate measurements on macrophages pooled from three animals are shown. Asterisks denote statistically significant differences ($P < 0.05$ by t test). (C) Primary cultures of peritoneal macrophages from 16-week-old female wild-type (lanes labeled with +) and *mGsta4* null mice (lanes labeled with −) were treated with LPS (100 ng/mL). After the indicated times, cells were solubilized in SDS sample buffer. Aliquots of the samples containing 32 μg of protein each were separated by 12% SDS−PAGE and electroblotted, and the blot was probed with an antibody against iNOS, followed by an antibody against β-actin (loading control).

phenotypes in genetically modified mice (*48, 49*). Although the reasons for the lack of the anticipated effect on 4-HNE levels in *mGsta4* null C57BL/6 mice were not investigated in the course of this work, it appears likely that, in comparison with 129/sv mice, C57BL/6 mice have a higher capacity to express or upregulate pathways of 4-HNE metabolism that do not depend on mGSTA4-4. Regardless of the underlying mechanism, the observed strain difference was fortuitous as it established that the level of 4-HNE correlates with malonyl-CoA levels and with fat accumulation. These results suggest that 4-HNE may be part of the mechanism that leads to an increase in malonyl-CoA levels. This hypothesis is strengthened by our finding that RNAi silencing of a 4-HNE-conjugating GST in the nematode *Caenorhabditis elegans* also leads to an increase in malonyl-CoA levels and to fat deposition (manuscript in preparation). Because *C. elegans* and mice diverged approximately one billion years ago (*50*), this result suggests that 4-HNE modulates a well-conserved biochemical process relevant to fat accumulation.

While persuasive in incriminating 4-HNE as the causative agent, the parallel response to disruption of 4-HNE-metabolizing GSTs in two widely divergent species may have an alternative interpretation: obesity could be triggered by a hypothetical shared substrate of the murine and nematode GSTs that is distinct from 4-HNE. It has been, however, shown that overexpression of murine aldose reductase AKR1B7 inhibits adipogenesis, and disruption of the same enzyme accelerates adipogenesis (*51*). Aldose reductases and GSTs are unrelated in their structure and type of catalyzed reaction, and it is unlikely that AKR1B7 and mGSTA4-4 share a substrate other than 4-HNE (perhaps with the exception of another α,β-unsaturated carbonyl compound). Moreover, exposure of yeast to 4-HNE also leads to fat deposition (*52*). The latter finding demonstrates that direct action of 4-HNE is sufficient to account for the observed biological end point (fat accumulation) in yeast and perhaps, as we postulate, also in mice. Taken together, the available data are most parsimoniously explained by a causative role of 4-HNE in malonyl-CoA-mediated accumulation of lipids.

The absence of elevated 4-HNE levels in *mGsta4* null C57BL/6 mice precludes the use of these animals for studies of how 4-HNE affects fat metabolism. For this reason, we focused our work on 129/sv mice in which an increase in the level of 4-HNE can be attained through a disruption of the *mGsta4* gene. It should be noted that 129/sv mice are generally considered to be less prone to developing insulin resistance and diet-induced obesity than C57BL/6 mice (*48, 49, 53*). Therefore, by examining 129/sv mice, we are not selecting a strain predisposed to exhibiting the phenotypes being studied.

The onset of obesity appears to precede hormonal changes in *mGsta4* null mice because the blood glucose level, albeit slightly higher than in wild-type animals, remains in the normal range, glucose tolerance is normal in both young and middle-aged mice (Figure 4), and insulin sensitivity does not differ between young *mGsta4* null and wild-type animals (Figure 5A,B). Insulin resistance becomes evident only in 50-week-old *mGsta4* null mice. Interestingly, there are large differences between responses of individual older animals to insulin (Figure 5D), suggesting that knockout mice begin to develop metabolic syndrome at an age of approximately 50 weeks, with some animals having progressed more than others in that pathology. These data indicate that the roots of obesity in *mGsta4* null mice are of metabolic rather than hormonal nature and that homeostatic and regulatory abnormalities such as metabolic syndrome may be secondary to the metabolic changes. This differentiates the *mGsta4* null mouse from other rodent obesity models such as *Lep*$^{ob/ob}$ or *Lepr*$^{db/db}$ (reviewed in ref *54*) in which the primary change is hormonal and may render *mGsta4* null animals particularly valuable for the elucidation of biochemical aspects of obesity.

The molecular mechanism by which 4-HNE may trigger fat accumulation can be divided into two stages: (1) how 4-HNE could cause an increase in the level of malonyl-CoA and (2) how an elevated level of malonyl-CoA leads to obesity. The latter process is well-understood. In lipogenic tissues such as WAT and liver, malonyl-CoA serves as the committed precursor of fatty acid synthesis. In oxidative tissues (mainly skeletal muscle but also liver), malonyl-CoA acts mostly as an inhibitor of carnitine palmitoyltransferase-1 (*55*). Inhibition of this enzyme prevents mitochondrial entry

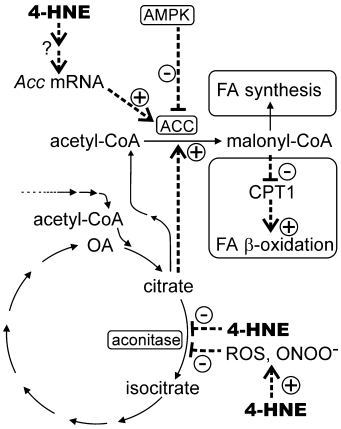

FIGURE 11: Scheme of the proposed mechanism by which an elevated level of 4-HNE leads to an increase in malonyl-CoA levels and to fat accumulation. See the text for details. Dashed arrows with a plus or minus sign denote activation or inhibition, respectively.

and thus β-oxidation of fatty acids. Both effects of malonyl-CoA increase the supply of fatty acids and lead to deposition of fat stores.

In contrast to malonyl-CoA-dependent fat accumulation, little is known about mechanisms by which 4-HNE can increase malonyl-CoA levels. The formation of malonyl-CoA is catalyzed by the enzyme ACC. As expected from its central role in energy sensing and fatty acid homeostasis, ACC is highly regulated both at the transcriptional and at the posttranscriptional levels (*42, 44*). Assuming that the higher level of *Acc2* mRNA in *mGsta4* null mice (Table 1) is reflected in an increase in the level of ACC2 protein and activity, this could contribute to the observed elevation of the level of malonyl-CoA, to a diminished rate of fatty acid β-oxidation, and thus to accumulation of triglycerides in these tissues. The exact mechanism by which 4-HNE may affect ACC2 expression is not known. However, 4-HNE has been shown to activate the stress kinases JNK and p38 (*6, 8, 56–58*) and thus modulate the expression of large sets of genes.

Although transcriptional regulation of ACC expression has been documented (reviewed in ref *44*), the predominant modalities of controlling the enzyme's activity are phosphorylation and allosteric regulation (*42, 44*). Citrate is a major allosteric activator of ACC. In the well-fed state, citrate is diverted from the TCA cycle to serve both as a precursor for acetyl-CoA (the substrate of ACC) and as an allosteric activator of ACC, thus promoting malonyl-CoA synthesis and, ultimately, storage of fat (Figure 11). In the TCA cycle, citrate is metabolized by aconitase. Although aconitase is not rate-limiting for the TCA cycle and small changes in aconitase activity would not be expected to affect the metabolite flux (*59*), a more substantial inhibition of aconitase results in an accumulation of citrate (*47*). Similarly, inhibition of the distal TCA cycle enzymes isocitrate dehydrogenase and α-ketoglutarate dehydrogenase, the latter a key regulatory step of the cycle (*59*), could lead to an accumulation of proximal substrates, including citrate. We have shown that mitochondrial aconitase is indeed partially inhibited in *mGsta4* null mice (Figure 8) and that citrate levels are increased in liver and skeletal muscle (Figure 9). We propose that the elevated level of citrate contributes to the activation of ACC. For example, if units of micromoles per gram of wet weight of tissue can be approximately equated with millimolar, the citrate concentration increases from 0.55 to 0.9 mM in livers of *mGsta4* null versus wild-type mice (Figure 9). Such a change in citrate level may result in a 30−40% increase in ACC activity (approximated from data presented in refs *60* and *61*), depending on the phosphorylation and perhaps polymerization state of the enzyme (*42, 44*). Higher ACC activity would contribute to malonyl-CoA-mediated fat accumulation.

There are several known mechanisms by which 4-HNE could lead to an inhibition of aconitase. The enzyme forms adducts with 4-HNE (*62, 63*). While it has not been reported whether this modification by 4-HNE is inhibitory, this appears likely because aconitase is inhibited by other α,β-unsaturated aldehydes such as acrolein (*64*) and possibly MDA (*35*). 4-HNE could also affect aconitase indirectly. 4-HNE is known to elicit oxidative stress and ROS production in cells (*65, 66*), and mitochondrial aconitase is very sensitive to ROS (*67, 68*). The recently reported inhibition of mitochondrial aconitase in cells treated with 4-HNE (*69*) could be due to direct or indirect effects of 4-HNE. In addition, aconitase could be inhibited by peroxynitrite ($ONOO^-$) (*70*) formed from macrophage-derived, diffusible nitric oxide (NO). Indeed, we observed a higher degree of tissue infiltration by macrophages (Table 1). Macrophage recruitment may be a consequence of chemotactic properties of 4-HNE. The compound is known to attract neutrophils at extremely low concentrations (*71*). In addition, 4-HNE induces the secretion of the monocyte chemoattractant protein-1 (MCP-1) by macrophages (*72*). MCP-1 is an attractant for several cell types, including T-lymphocytes (*73*) and the macrophage precursor cells, monocytes (*74*). Finally, macrophages isolated from *mGsta4* null mice are hyper-responsive in that they produce more ROS and more nitric oxide upon activation (Figure 10). Because there is no significant infiltration of WAT by macrophages at 16 weeks of age (Table 1), macrophage-mediated effects do not explain aconitase inhibition in young animals but could contribute at later stages of life. Isocitrate dehydrogenase and α-ketoglutarate dehydrogenase are also targets for 4-HNE inhibition (*75–78*).

The evidence for transcriptional and allosteric regulation of ACC does not suggest that these two mechanisms account for the entire effect of 4-HNE on malonyl-CoA levels. ACC is subject to allosteric regulation by multiple metabolites. In addition to citrate, these include other intermediates of the TCA cycle, fatty acyl-CoA, and malonyl-CoA itself. Phosphorylation by several kinases, particularly by AMPK, constitutes another important modality of acute ACC regulation; there is a complex interplay between allosteric regulation and the effects of phosphorylation (*44*). Further work will be needed to determine whether 4-HNE modulates ACC regulation by mechanisms other than those we have already identified.

In our experimental model, the proposed chain of events (increase in the 4-HNE level, increase in ACC activity, accumulation of malonyl-CoA, and fat deposition) is initiated by an experimental intervention (*mGsta4* gene knockout). However, we propose that this mechanism is also part of normal physiology. We base this assertion on recent findings by others that diet-induced obesity results in an overproduction of 4-HNE and in a decreased abundance of the mGSTA4-4 protein (*13*). Combined, our observations and those of Grimsrud et al. (*13*) indicate that obesity and 4-HNE

are mutually inductive and are likely to result in a positive feedback loop. Regardless of how it is initiated, obesity is characterized by a chronic, low-level inflammatory state (*9*) and infiltration of WAT by macrophages (*10–12*). This leads to a pro-oxidative state and loss of mGSTA4-4 (*13*). The resulting compromised metabolism causes an elevation of 4-HNE levels, especially in the face of an increased level of lipid peroxidation linked to the inflammatory state. By mechanisms described in this report, the excessive 4-HNE leads to obesity, thus closing the cycle. It should be noted that this positive feedback loop can be entered either by disruption of the *mGsta4* gene (our work) or by diet-induced obesity (*13*); in either case, the result would be low (or absent) mGSTA4-4 activity, an excess of 4-HNE, and a self-sustaining obese state.

The proposed obesity/inflammation/4-HNE positive feedback mechanism would promote and perpetuate adiposity as long as food is available, a process that was adaptive throughout evolution but became maladaptive in modern industrial societies. Such a mechanism may contribute to the strong pro-adipose bias of an organism's regulatory circuits. On the other hand, breaking this cycle could be useful in weight loss regimens.

In summary, we provide evidence in favor of a model in which an experimentally increased tissue level of 4-HNE leads to an elevation of the level of malonyl-CoA via higher expression of ACC2 and/or allosteric activation of ACC; other mechanisms, such as phosphorylation, could also mediate the effects of 4-HNE. By well-known pathways, the excessive malonyl-CoA causes fat accumulation and obesity in the animal. The observed effects can be explained by metabolic mechanisms, and in fact, they precede hormone-linked changes such as insulin resistance. The *mGsta4* null mouse model is therefore suitable for the exploration of biochemical aspects of obesity. At the same time, our work in conjunction with published results by others (*13*) suggests the existence of a positive feedback loop involving 4-HNE and perpetuating obesity as long as food is available. An understanding of this essentially metabolic regulatory circuit that assures a self-sustaining nature of the obese state should be helpful in devising treatments to alleviate the condition.

REFERENCES

1. Gutteridge, J. M. C., and Halliwell, B. (1990) The measurement and mechanism of lipid peroxidation in biological systems. *Trends Biochem. Sci. 15*, 129–135.
2. Schneider, C., Porter, N. A., and Brash, A. R. (2004) Autoxidative transformation of chiral ω6 hydroxy linoleic and arachidonic acids to chiral 4-hydroxy-2*E*-nonenal. *Chem. Res. Toxicol. 17*, 937–941.
3. Sun, M., and Salomon, R. G. (2004) Oxidative fragmentation of hydroxy octadecadienoates generates biologically active γ-hydroxyalkenals. *J. Am. Chem. Soc. 126*, 5699–5708.
4. Esterbauer, H., Schaur, R. J., and Zollner, H. (1991) Chemistry and biochemistry of 4-hydroxynonenal, malonaldehyde and related aldehydes. *Free Radical Biol. Med. 11*, 81–128.
5. Poli, G., Schaur, R. J., Siems, W. G., and Leonarduzzi, G. (2007) 4-Hydroxynonenal: A membrane lipid oxidation product of medicinal interest. *Med. Res. Rev.* (in press).
6. Petersen, D. R., and Doorn, J. A. (2004) Reactions of 4-hydroxynonenal with proteins and cellular targets. *Free Radical Biol. Med. 37*, 937–945.
7. Leonarduzzi, G., Robbesyn, F., and Poli, G. (2004) Signaling kinases modulated by 4-hydroxynonenal. *Free Radical Biol. Med. 37*, 1694–1702.
8. Dwivedi, S., Sharma, A., Patrick, B., Sharma, R., and Awasthi, Y. C. (2007) Role of 4-hydroxynonenal and its metabolites in signaling. *Redox Rep. 12*, 4–10.
9. Wellen, K. E., and Hotamisligil, G. S. (2003) Obesity-induced inflammatory changes in adipose tissue. *J. Clin. Invest. 112*, 1785–1788.
10. Weisberg, S. P., McCann, D., Desai, M., Rosenbaum, M., Leibel, R. L., and Ferrante, A. W., Jr. (2003) Obesity is associated with macrophage accumulation in adipose tissue. *J. Clin. Invest. 112*, 1796–1808.
11. Xu, H., Barnes, G. T., Yang, Q., Tan, G., Yang, D., Chou, C. J., Sole, J., Nichols, A., Ross, J. S., Tartaglia, L. A., and Chen, H. (2003) Chronic inflammation in fat plays a crucial role in the development of obesity-related insulin resistance. *J. Clin. Invest. 112*, 1821–1830.
12. Cinti, S., Mitchell, G., Barbatelli, G., Murano, I., Ceresi, E., Faloia, E., Wang, S. L., Greenberg, A. S., and Obin, M. S. (2005) Adipocyte death defines macrophage localization and function in adipose tissue of obese mice and humans. *J. Lipid Res. 46*, 2347–2355.
13. Grimsrud, P. A., Picklo Sr, M. J., Griffin, T. J., and Bernlohr, D. A. (2007) Carbonylation of adipose proteins in obesity and insulin resistance: Identification of adipocyte fatty acid-binding protein as a cellular target of 4-hydroxynonenal. *Mol. Cell. Proteomics 6*, 624–637.
14. Esterbauer, H. (1993) Cytotoxicity and genotoxicity of lipid-oxidation products. *Am. J. Clin. Nutr. 57*, 779S–786S.
15. Spiteller, G. (2007) The important role of lipid peroxidation processes in aging and age dependent diseases. *Mol. Biotechnol. 37*, 5–12.
16. Hayes, J. D., Flanagan, J. U., and Jowsey, I. R. (2005) Glutathione transferases. *Annu. Rev. Pharmacol. Toxicol. 45*, 51–88.
17. Zimniak, P., and Singh, S. P. (2006) Families of glutathione transferases, in *Toxicology of glutathione transferases* (Awasthi, Y. C., Ed.) pp 11–26, CRC Press, Boca Raton, FL.
18. Awasthi, S., Cheng, J.-Z., Singhal, S. S., Zhao, T., Saini, M. K., Pandya, U., Clark-Wronski, J., Zimniak, P., and Awasthi, Y. C. (2001) Physiological substrates of glutathione S-transferases. *Chem.-Biol. Interact. 133*, 217–223.
19. Zimniak, P., Singhal, S. S., Srivastava, S. K., Awasthi, S., Sharma, R., Hayden, J. B., and Awasthi, Y. C. (1994) Estimation of genomic complexity, heterologous expression, and enzymatic characterization of mouse glutathione S-transferase mGSTA4-4 (GST 5.7). *J. Biol. Chem. 269*, 992–1000.
20. Alin, P., Danielson, U. H., and Mannervik, B. (1985) 4-Hydroxyalk-2-enals are substrates for glutathione transferase. *FEBS Lett. 179*, 267–270.
21. Jensson, H., Guthenberg, C., Alin, P., and Mannervik, B. (1986) Rat glutathione transferase 8-8, an enzyme efficiently detoxifying 4-hydroxyalk-2-enals. *FEBS Lett. 203*, 207–209.
22. Hubatsch, I., Ridderstrom, M., and Mannervik, B. (1998) Human glutathione transferase A4-4: An Alpha class enzyme with high catalytic efficiency in the conjugation of 4-hydroxynonenal and other genotoxic products of lipid peroxidation. *Biochem. J. 330*, 175–179.
23. Bruns, C. M., Hubatsch, I., Ridderstrom, M., Mannervik, B., and Tainer, J. A. (1999) Human glutathione transferase A4-4 crystal structures and mutagenesis reveal the basis of high catalytic efficiency with toxic lipid peroxidation products. *J. Mol. Biol. 288*, 427–439.
24. Xiao, B., Singh, S. P., Nanduri, B., Awasthi, Y. C., Zimniak, P., and Ji, X. (1999) Crystal structure of a murine glutathione S-transferase in complex with a glutathione conjugate of 4-hydroxynon-2-enal in one subunit and glutathione in the other: Evidence of signaling across the dimer interface. *Biochemistry 38*, 11887–11894.
25. Engle, M. R., Singh, S. P., Czernik, P. J., Gaddy, D., Montague, D. C., Ceci, J. D., Yang, Y., Awasthi, S., Awasthi, Y. C., and Zimniak, P. (2004) Physiological role of mGSTA4-4, a glutathione S-transferase metabolizing 4-hydroxynonenal: Generation and analysis of mGsta4 null mouse. *Toxicol. Appl. Pharmacol. 194*, 296–308.
26. Gerard-Monnier, D., Erdelmeier, I., Regnard, K., Moze-Henry, N., Yadan, J. C., and Chaudiere, J. (1998) Reactions of 1-methyl-2-phenylindole with malondialdehyde and 4-hydroxyalkenals. Analytical applications to a colorimetric assay of lipid peroxidation. *Chem. Res. Toxicol. 11*, 1176–1183.

27. Wollenberger, A., Ristau, O., and Schoffa, G. (1960) Eine einfache Technik der sehr schnellen Abkühlung grösserer Gewebestücke. *Pfluegers Arch. Gesamte Physiol. Menschen Tiere 270*, 399–412.
28. Gree, R., Tourbah, H., and Carrie, R. (1986) Fumaraldehyde monodimethyl acetal: An easily accessible and versatile intermediate. *Tetrahedron Lett. 27*, 4983–4986.
29. Chandra, A., and Srivastava, S. K. (1997) A synthesis of 4-hydroxy-2-trans-nonenal and 4-(^{3}H) 4-hydroxy-2-trans-nonenal. *Lipids 32*, 779–782.
30. Lazzarino, G., Amorini, A. M., Fazzina, G., Vagnozzi, R., Signoretti, S., Donzelli, S., Di Stasio, E., Giardina, B., and Tavazzi, B. (2003) Single-sample preparation for simultaneous cellular redox and energy state determination. *Anal. Biochem. 322*, 51–59.
31. Möllering, H., and Gruber, W. (1966) Determination of citrate with citrate lyase. *Anal. Biochem. 17*, 369–376.
32. Chomczynski, P., and Sacchi, N. (1987) Single-step method of RNA isolation by acid guanidinium thiocyanate-phenol-chloroform extraction. *Anal. Biochem. 162*, 156–159.
33. Wang, X., and Seed, B. (2003) A PCR primer bank for quantitative gene expression analysis. *Nucleic Acids Res. 31*, e154.
34. Rebrin, I., and Sohal, R. S. (2004) Comparison of thiol redox state of mitochondria and homogenates of various tissues between two strains of mice with different longevities. *Exp. Gerontol. 39*, 1513–1519.
35. Yarian, C. S., Rebrin, I., and Sohal, R. S. (2005) Aconitase and ATP synthase are targets of malondialdehyde modification and undergo an age-related decrease in activity in mouse heart mitochondria. *Biochem. Biophys. Res. Commun. 330*, 151–156.
36. Melnick, J. Z., Preisig, P. A., Moe, O. W., Srere, P., and Alpern, R. J. (1998) Renal cortical mitochondrial aconitase is regulated in hypo- and hypercitraturia. *Kidney Int. 54*, 160–165.
37. Tiwari, M. M., Messer, K. J., and Mayeux, P. R. (2006) Inducible nitric oxide synthase and apoptosis in murine proximal tubule epithelial cells. *Toxicol. Sci. 91*, 493–500.
38. Wu, R., Ma, C.-X., Zhao, W., and Casella, G. (2003) Functional mapping for quantitative trait loci governing growth rates: A parametric model. *Physiol. Genomics 14*, 241–249.
39. Standaert, M. L., Bandyopadhyay, G., Galloway, L., Soto, J., Ono, Y., Kikkawa, U., Farese, R. V., and Leitges, M. (1999) Effects of knockout of the protein kinase C β gene on glucose transport and glucose homeostasis. *Endocrinology 140*, 4470–4477.
40. Terauchi, Y., Matsui, J., Suzuki, R., Kubota, N., Komeda, K., Aizawa, S., Eto, K., Kimura, S., Nagai, R., Tobe, K., Lienhard, G. E., and Kadowaki, T. (2003) Impact of genetic background and ablation of insulin receptor substrate (IRS)-3 on IRS-2 knock-out mice. *J. Biol. Chem. 278*, 14284–14290.
41. Kido, Y., Philippe, N., Schaffer, A. A., and Accili, D. (2000) Genetic modifiers of the insulin resistance phenotype in mice. *Diabetes 49*, 589–596.
42. Munday, M. R. (2002) Regulation of mammalian acetyl-CoA carboxylase. *Biochem. Soc. Trans. 30*, 1059–1064.
43. Harwood, H. J., Jr. (2004) Acetyl-CoA carboxylase inhibition for the treatment of metabolic syndrome. *Curr. Opin. Invest. Drugs 5*, 283–289.
44. Barber, M. C., Price, N. T., and Travers, M. T. (2005) Structure and regulation of acetyl-CoA carboxylase genes of metazoa. *Biochim. Biophys. Acta 1733*, 1–28.
45. Abu-Elheiga, L., Matzuk, M. M., Abo-Hashema, K. A., and Wakil, S. J. (2001) Continuous fatty acid oxidation and reduced fat storage in mice lacking acetyl-CoA carboxylase 2. *Science 291*, 2613–2616.
46. Oh, W., Abu-Elheiga, L., Kordari, P., Gu, Z., Shaikenov, T., Chirala, S. S., and Wakil, S. J. (2005) Glucose and fat metabolism in adipose tissue of acetyl-CoA carboxylase 2 knockout mice. *Proc. Natl. Acad. Sci. U.S.A. 102*, 1384–1389.
47. Hassel, B., Sonnewald, U., Unsgard, G., and Fonnum, F. (1994) NMR spectroscopy of cultured astrocytes: Effects of glutamine and the gliotoxin fluorocitrate. *J. Neurochem. 62*, 2187–2194.
48. Clee, S. M., and Attie, A. D. (2007) The genetic landscape of type 2 diabetes in mice. *Endocr. Rev. 28*, 48–83.
49. Linder, C. C. (2006) Genetic variables that influence phenotype. *ILAR J. 47*, 132–140.
50. Blair, J. E., Shah, P., and Hedges, S. B. (2005) Evolutionary sequence analysis of complete eukaryote genomes. *BMC Bioinf. 6*, 53.
51. Tirard, J., Gout, J., Lefrancois-Martinez, A. M., Martinez, A., Begeot, M., and Naville, D. (2007) A novel inhibitory protein in adipose tissue: The aldo-keto-reductase AKR1B7. Its role in adipogenesis. *Endocrinology 148*, 1996–2005.
52. Wonisch, W., Zellnig, G., Kohlwein, S. D., Schaur, R. J., Bilinski, T., Tatzber, F., and Esterbauer, H. (2001) Ultrastructural analysis of HNE-treated *Saccharomyces cerevisiae* cells reveals fragmentation of the vacuole and an accumulation of lipids in the cytosol. *Cell Biochem. Funct. 19*, 59–64.
53. Almind, K., and Kahn, C. R. (2004) Genetic determinants of energy expenditure and insulin resistance in diet-induced obesity in mice. *Diabetes 53*, 3274–3285.
54. Imai, Y., and Ahima, R. S. (2005) Rodents as genetic models of obesity. *Drug Discovery Today: Dis. Models 2*, 165–175.
55. Borthwick, K. L., Jackson, V. N., Price, N. T., and Zammit, V. A. (2006) The mitochondrial intermembrane loop region of rat carnitine palmitoyltransferase 1A is a major determinant of its malonyl-CoA sensitivity. *J. Biol. Chem. 281*, 32946–32952.
56. Leonarduzzi, G., Arkan, M. C., Basaga, H., Chiarpotto, E., Sevanian, A., and Poli, G. (2000) Lipid oxidation products in cell signaling. *Free Radical Biol. Med. 28*, 1370–1378.
57. Awasthi, Y. C., Sharma, R., Cheng, J. Z., Yang, Y., Sharma, A., Singhal, S. S., and Awasthi, S. (2003) Role of 4-hydroxynonenal in stress-mediated apoptosis signaling. *Mol. Aspects Med. 24*, 219–230.
58. Kutuk, O., and Basaga, H. (2007) Apoptosis signalling by 4-hydroxynonenal: A role for JNK-c-Jun/AP-1 pathway. *Redox Rep. 12*, 30–34.
59. Wu, F., Yang, F., Vinnakota, K. C., and Beard, D. A. (2007) Computer modeling of mitochondrial tricarboxylic acid cycle, oxidative phosphorylation, metabolite transport, and electrophysiology. *J. Biol. Chem. 282*, 24525–24537.
60. Thampy, K. G., and Wakil, S. J. (1985) Activation of acetyl-CoA carboxylase. Purification and properties of a Mn^{2+}-dependent phosphatase. *J. Biol. Chem. 260*, 6318–6323.
61. Witters, L. A., Moriarity, D., and Martin, D. B. (1979) Regulation of hepatic acetyl coenzyme A carboxylase by insulin and glucagon. *J. Biol. Chem. 254*, 6644–6649.
62. Hussain, S. N., Matar, G., Barreiro, E., Florian, M., Divangahi, M., and Vassilakopoulos, T. (2006) Modifications of proteins by 4-hydroxy-2-nonenal in the ventilatory muscles of rats. *Am. J. Physiol. 290*, L996–L1003.
63. Stevens, S. M., Jr., Rauniyar, N., and Prokai, L. (2007) Rapid characterization of covalent modifications to rat brain mitochondrial proteins after ex vivo exposure to 4-hydroxy-2-nonenal by liquid chromatography-tandem mass spectrometry using data-dependent and neutral loss-driven MS^3 acquisition. *J. Mass Spectrom. 42*, 1599–1605.
64. Luo, J., and Shi, R. (2005) Acrolein induces oxidative stress in brain mitochondria. *Neurochem. Int. 46*, 243–252.
65. Uchida, K. (2003) 4-Hydroxy-2-nonenal: A product and mediator of oxidative stress. *Prog. Lipid Res. 42*, 318–343.
66. Lee, J. Y., Jung, G. Y., Heo, H. J., Yun, M. R., Park, J. Y., Bae, S. S., Hong, K. W., Lee, W. S., and Kim, C. D. (2006) 4-Hydroxynonenal induces vascular smooth muscle cell apoptosis through mitochondrial generation of reactive oxygen species. *Toxicol. Lett. 166*, 212–221.
67. Gardner, P. R. (2002) Aconitase: Sensitive target and measure of superoxide. *Methods Enzymol. 349*, 9–23.
68. Yan, L. J., Levine, R. L., and Sohal, R. S. (1997) Oxidative damage during aging targets mitochondrial aconitase. *Proc. Natl. Acad. Sci. U.S.A. 94*, 11168–11172.
69. Raza, H., John, A., Brown, E. M., Benedict, S., and Kambal, A. (2007) Alterations in mitochondrial respiratory functions, redox metabolism and apoptosis by oxidant 4-hydroxynonenal and antioxidants curcumin and melatonin in PC12 cells. *Toxicol. Appl. Pharmacol. 226*, 161–168.
70. Han, D., Canali, R., Garcia, J., Aguilera, R., Gallaher, T. K., and Cadenas, E. (2005) Sites and mechanisms of aconitase inactivation by peroxynitrite: Modulation by citrate and glutathione. *Biochemistry 44*, 11986–11996.
71. Rossi, M. A., Di Mauro, C., Esterbauer, H., Fidale, F., and Dianzani, M. U. (1994) Activation of phosphoinositide-specific phospholipase C of rat neutrophils by the chemotactic aldehydes 4-hydroxy-2,3-trans-nonenal and 4-hydroxy-2,3-trans-octenal. *Cell Biochem. Funct. 12*, 275–280.
72. Nitti, M., Domenicotti, C., d'Abramo, C., Assereto, S., Cottalasso, D., Melloni, E., Poli, G., Biasi, F., Marinari, U. M., and Pronzato, M. A. (2002) Activation of PKC-β isoforms mediates HNE-induced MCP-1 release by macrophages. *Biochem. Biophys. Res. Commun. 294*, 547–552.

73. Larche, M., Robinson, D. S., and Kay, A. B. (2003) The role of T lymphocytes in the pathogenesis of asthma. *J. Allergy Clin. Immunol. 111*, 450–463.
74. Jiang, Y., Beller, D. I., Frendl, G., and Graves, D. T. (1992) Monocyte chemoattractant protein-1 regulates adhesion molecule expression and cytokine production in human monocytes. *J. Immunol. 148*, 2423–2428.
75. Benderdour, M., Charron, G., DeBlois, D., Comte, B., and Des Rosiers, C. (2003) Cardiac mitochondrial $NADP^+$-isocitrate dehydrogenase is inactivated through 4-hydroxynonenal adduct formation: An event that precedes hypertrophy development. *J. Biol. Chem. 278*, 45154–45159.
76. Benderdour, M., Charron, G., Comte, B., Ayoub, R., Beaudry, D., Foisy, S., Deblois, D., and Des Rosiers, C. (2004) Decreased cardiac mitochondrial $NADP^+$-isocitrate dehydrogenase activity and expression: A marker of oxidative stress in hypertrophy development. *Am. J. Physiol. 287*, H2122–H2131.
77. Yang, J. H., Yang, E. S., and Park, J. W. (2004) Inactivation of $NADP^+$-dependent isocitrate dehydrogenase by lipid peroxidation products. *Free Radical Res. 38*, 241–249.
78. Humphries, K. M., and Szweda, L. I. (1998) Selective inactivation of α-ketoglutarate dehydrogenase and pyruvate dehydrogenase: Reaction of lipoic acid with 4-hydroxy-2-nonenal. *Biochemistry 37*, 15835–15841.
79. Fleige, S., Walf, V., Huch, S., Prgomet, C., Sehm, J., and Pfaffl, M. W. (2006) Comparison of relative mRNA quantification models and the impact of RNA integrity in quantitative real-time RT-PCR. *Biotechnol. Lett. 28*, 1601–1613.
80. Erdelmeier, I., Gerard-Monnier, D., Yadan, J. C., and Chaudiere, J. (1998) Reactions of N-methyl-2-phenylindole with malondialdehyde and 4-hydroxyalkenals. Mechanistic aspects of the colorimetric assay of lipid peroxidation. *Chem. Res. Toxicol. 11*, 1184–1194.

BI702124U